Corrosion behaviour of brazing material AA4343

S. Tierce, N. Pébère, C. Blanc, C. Casenave, G. Mankowski and H. Robidou

CIRIMAT, UMR CNRS 5085, ENSIACET, 31077 Toulouse Cedex 4, France
Valeo Engine Cooling, BP14, 72210 La Suze sur Sarthe, France

Abstract

This paper is part of a work devoted to corrosion of brazed AA4343/AA3003/AA4343 materials on water side of automotive heater cores. The microstructure of the superficial resolidified AA4343 brazing material has been previously characterised [1] and [2]. It is composed of large (Al) grains separated by valleys containing multiphase deposits of (Al), Si and α-Al(Mn,Fe)Si. The present study focuses on its electrochemical behaviours in neutral water–ethylene glycol mixtures at different temperatures with and without chloride ions. Three types of behaviour are revealed: (i) passivation, (ii) defective passivation and (iii) pitting corrosion at the corrosion potential. The defective passivation is investigated in greater depth. The results show that Si needles do not participate in the corrosion progress whereas the α-Al(Mn,Fe)Si particles are preferential sites for corrosion attacks. α-Al(Mn,Fe)Si particle/matrix interactions are responsible of the defective passivation at valleys level where the α-Al(Mn,Fe)Si phase particles are mainly concentrated. Increasing the temperature enhances this reactivity whereas addition of ethylene glycol decreases it and favours a transition from defective passivation to passivation for ethylene glycol content higher than 55%.

Keywords: Corrosion; Brazing; AA4343 cladding; α-Al(Fe,Mn)Si phase; Water–ethylene glycol mixtures

1. Introduction

Aluminium is a light metal which presents interesting properties for heat exchanger applications (low density, good thermal conductivity, satisfactory mechanical properties and relatively good corrosion resistance). Since the middle of the 1990s, the trend with automotive heat exchangers has been to replace mechanical assembly by brazing of aluminium alloys. Most of the brazed aluminium sheets consist of multi-layer materials composed of a 3XXX core alloy clad on one or both sides with a 4XXX alloy.

In this study, the parts to be brazed were composed of AA4343/AA3003[a]/AA4343 sandwich sheets where AA3003[a] is an Al–Mn base alloy and AA4343 an Al–Si base alloy. The brazing process is based on the difference in the melting points between the two alloys. A gap of about 30 °C exists between the liquidus of the cladding and the solidus of the core material. During the brazing process, the parts to be assembled are heated for a short duration at a temperature between the melting temperatures of the two alloys. To favour the wettability of the melted cladding at the surface of the material, Nocolok® fluxing [3] is used to remove the natural oxide layer covering the aluminium alloys.

Brazing modifies the geometry and the microstructure of the cladding as well as the microstructure of the core [1], [2], [3], [4], [5], [6], [7], [8], [9], [10] and [11]. In previous studies [1] and [2], a synthesis of solidification and phase transformations occurring during brazing was presented with particular attention paid to phase identification. Resolidification of AA4343 leads to the formation of both brazed joints at the contact points between the different parts and of a residual thin layer of cladding covering the flat surfaces of the parts away from the brazing joints. Multiphase deposits of (Al), α-Al(Fe,Mn)Si and Si were observed in these areas. After this previously published microstructural study, the aim of the present paper was to investigate the corrosion behaviour of the residual cladding in water–ethylene glycol (EG) mixtures since water and EG are the main components of the coolants used in automotive cooling loop.

Several studies have been devoted to the corrosion behaviour of brazed Al–Si base alloys. In studies devoted to the air-side corrosion sensitivity of these materials, Scott et al. [12] and Isobe et al. [13] considered that noble Si needles had a detrimental effect on the corrosion resistance of the residual cladding. Scott et al. [12] studied the corrosion behaviour of these materials with sea water acetic acid test (SWAAT); whereas, Isobe et al. [13] used copper accelerated salt spray (CASS) and acetic acid salt spray (AASS) tests. They observed that Si needles acted as active cathodes while the surrounding aluminium dissolved.

Al–Si alloys were also studied for other technological applications. In acidic or neutral solutions, it has been shown that Si particles did not have a detrimental effect on the corrosion resistance of aluminium alloys [14] and [15]. Some papers devoted to the corrosion of brazed aluminium heat exchangers [16] and [17] also agree with this point stating that the cathodic reaction mentioned by Scott et al. [12] and Isobe et al. [13] did not occur on Si needles. Kuroda and Tohma [16] and Meijers [17] determined that the oxygen reduction current density on silicon is too low to anodically polarise aluminium. From their point of view, the corrosion susceptibility of the residual cladding arises from a higher sensitivity to pitting of the eutectic (Al) in solutions containing chloride. This has been explained by a lower pitting potential for eutectic (Al) than for the primary (Al).

Few papers have discussed the role of the α-Al(Fe,Mn)Si phase precipitates on the corrosion resistance of the residual cladding. Isobe et al. [13] considered that large Al–Mn–Fe–Si intermetallic compounds had a cathodic behaviour similar to that of Si needles. In an electrochemical study dedicated to the behaviour of aluminium-based intermetallics containing iron, Nisançiöglu [18] studied the electrochemical behaviour of α-Al(Fe,Mn)Si particles isolated from their (Al) matrix. When the α-Al(Fe,Mn)Si phase particles were immersed in 0.1 M NaOH solution, Fe, Mn and Si enrichment of the surface of the particle was observed. Due to the evolution of the chemical composition of their surface, Nisançiöglu estimated that the particles tended to passivate and to become cathodic sites. However, Nisançiöglu and Lunder [19] postulated that silica enrichment of the surface significantly reduced the rate of the cathodic reaction on these particles. They emphasised the complexity of the phenomena occurring in the presence of multi-component intermetallics and did not evoke the influence of possible particle/matrix interactions on the reactivity observed for the α-Al(Fe,Mn)Si phase particles. The ambiguity of the behaviour of Si reported in the literature demonstrates the need to clarify the role of both Si and α-Al(Fe,Mn)Si heterogeneities on the

corrosion behaviour of the residual cladding. Due to the context of the study, it is also necessary to take into account the influence of parameters related to cooling liquids such as ethylene glycol content, temperature and addition of chloride ions. In the present work, electrochemical measurements (plots of potentiodynamic polarisation curves) were combined with microscope observations of the metal surface (optical microscope (OM) and scanning electron microscope (SEM)). In addition, phase shifting interferometric microscope (PSIM) observations were performed to study the reactivity of the intermetallic particles and secondary ion mass spectroscopy (SIMS) analyses were carried out to determine the nature of the corrosion products observed around the α-Al(Fe,Mn)Si particles.

2. Experimental

The brazed material studied was from heater core tubes. The average composition of the core alloy (AA3003[a]) and of the cladding (AA4343) before brazing is given in Table 1. The microstructural modifications occurring in the aluminium alloys during brazing has been investigated previously [1] and [2]. Fig. 1 and Fig. 2 recall the microstructure of the brazed material and more particularly that of the residual cladding. Fig. 1 shows an optical micrograph of a section of a brazed part after etching with Keller's reagent. The core material (AA3003[a]) is on the left of the micrograph. A “band of dense precipitates” (BDP) resulting from the diffusion of silicon from the melted cladding into the core appears in grey contrast. In this area, Si enrichment induces solid state precipitation of the α-Al(Fe,Mn)Si phase. The thin white film (5–10 μm) observed on the right of the micrograph is the residual resolidified Al–Si cladding. Fig. 2 presents SEM observations of the surface of the residual cladding. Large (Al) grains separated by valleys containing multiphase deposits of (Al), Si and α-Al(Fe,Mn)Si are observed (Fig. 2(a)). α-Al(Fe,Mn)Si plate-like precipitates are also observed on the surface embedded within the (Al) grains (Fig. 2(b)). The average area of residual cladding covered by α-Al(Fe,Mn)Si particles is between 1 and 2% of the total surface area. For the electrochemical measurements, the brazed sheet sample was electrically connected by soldering a copper wire. The assembly obtained was hot embedded in a phenolic resin. Then, the residual cladding electrode obtained was cleaned with a piece of felt and immersed in an ultrasonic bath containing water to remove the residual Nocolok® salts. A varnish was finally applied at the border of the electrode to prevent cavernous corrosion at the electrode/resin interface.

Table 1.

Chemical composition (wt.%) of aluminium alloys before brazing

	Si	Mn	Fe	Cu	Zn	Al
AA3003[a]	0.08	1.10	0.16	0.19	0.1	Bal.
AA4343	7.86	0.01	0.09	0.11	0.09	Bal.

[a] Modified AA3003.

Fig. 1. Optical microscope observation of a section of the brazed material (after a 60 s Keller's etching).

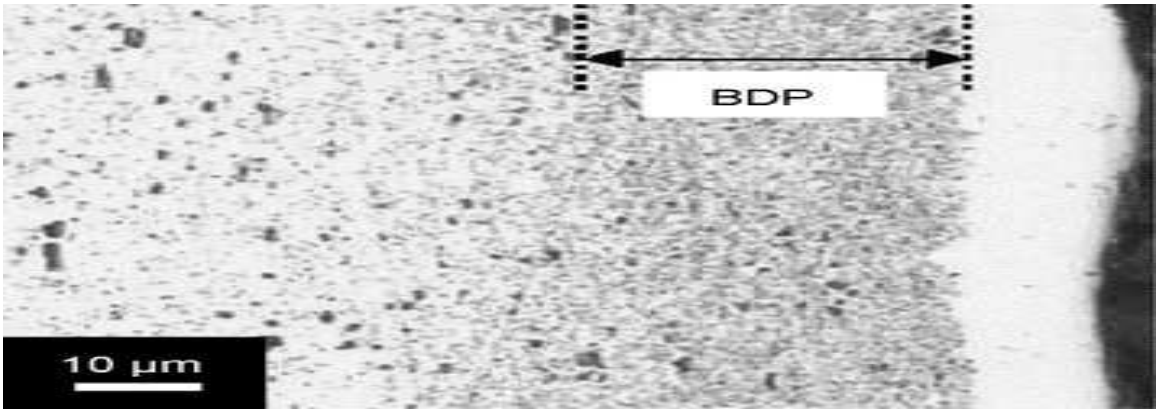

Fig. 2. Scanning electron microscope observations of the surface of the resolidified cladding showing (a) the microstructure in the valleys between the (Al) grains (15 kV, Wd = 19 mm) and (b) the plate-like particles of α-Al(Fe,Mn)Si phase embedded in the (Al) grains (15 kV, Wd = 19 mm, tilt 45°).

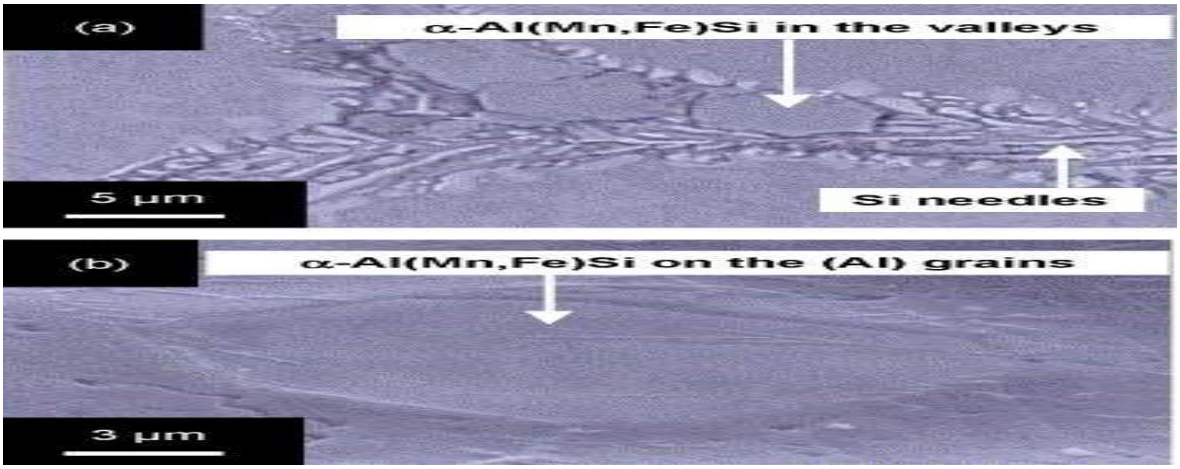

A three-electrode cell was used for the experiments: the residual cladding working electrode, a platinum plate auxiliary electrode and a saturated K_2SO_4/Hg_2SO_4 reference electrode (SSE). Electrochemical measurements were performed with an Autolab PGSTAT12 apparatus. Each experiment began with immersion of the residual cladding electrode at open circuit potential (OCP) for 1 h followed by polarisation from −1.5 to −0.2 V/SSE at a potential sweep rate of 1 V/h. Potentiodynamic polarisation curves were first obtained in 0.1 M Na_2SO_4 solutions open to air. Sodium sulphate was chosen to increase the conductivity of the solution and for its low corrosiveness toward aluminium alloys. Experiments were performed at different temperatures (10, 50 and 90 °C) in different 0.1 M Na_2SO_4 water–ethylene glycol (EG) mixtures (0, 30, 60 and 80 wt.% EG). Then, similar measurements were carried out in 0.1 M Na_2SO_4 + 0.01 M NaCl solutions to simulate the possible introduction of chloride ions in the cooling loop. Concerning the properties of the solutions, the conductivity was close to 10 mS cm^{-1} whereas the pH of the 0.1 M Na_2SO_4 solutions linearly varied in the range of 5.8 for 0 wt.% EG to 7 for 80 wt.% EG. These values of pH, included in the passivation domain of pure aluminium [20], are representative of the values encountered in the coolants.

To understand the corrosion mechanisms, complementary electrochemical measurements are required, particularly on the α-Al(Fe,Mn)Si phase particles separated from their matrix. The method envisaged in the present study largely drew its inspiration from the work of Nisançiöglu [18]. In the study devoted to the electrochemical behaviour of aluminium-base intermetallics containing iron, Nisançiöglu presented a protocol to prepare electrodes of α-Al(Fe,Mn)Si phase from a cast alloy containing α-Al(Fe,Mn)Si phase particles embedded in an aluminium matrix. From a polished surface, he dissolved the matrix by immersing the specimen in 0.5 M NaOH solution. The intermetallics were slightly attacked at the outset but they rapidly formed dark passivating layers which prevented further dissolution. When the aluminium matrix had been sufficiently attacked, the surface was recast in epoxy and polished through 0.05 μm alumina. He obtained active electrode areas of 0.3–0.5 cm^2. In the present work, the protocol applied was exactly the same. The electrode obtained was a little different from that obtained by Nisançiöglu due to the small surface of the α-Al(Fe,Mn)Si phase particles and the presence of silicon needles in the residual cladding. As silicon does not dissolve in the 0.5 M NaOH solution, some silicon needles remained on the working electrode. Their presence should have little effect on the measurements due to their low conductivity which limits their contribution to the current density measured. The low proportion and the small size of the precipitates of α-Al(Fe,Mn)Si phase in the residual cladding yielded a very small working area, about 0.2 mm^2 as measured with an image analysis software. Polarisation curves and long-term open circuit potential measurements obtained for the specimens were compared to results obtained for pure aluminium.

The surface of the residual cladding was examined before and after immersion in the solutions by optical microscopy (OM) and scanning electron microscopy (SEM) using a LEO 435 VP apparatus.

Phase shifting interferometric microscopy (PSIM) was used to study the evolution of the profiles of the surface around the heterogeneities of the material. This technique is based on classical interferometry with the particularity that four images were acquired for the same surface by varying the distance between the sample and the interferometric objective ($\Delta = \lambda/4$). Each image was recorded with a CCD camera and stored on a hard disk. Data processing consisted of determining the height of each point $h(x,y)$ on the image knowing the four intensities measured with four different optical path lengths. The vertical resolution is approximately 1 nm. The lateral resolution is that of a conventional objective around 0.4 μm.

For PSIM experiments, samples need to be mirror polished (alumina grain size 0.25 μm). 3D profiles were plotted before and after 90 min of immersion in deionised water without any additives (pH 5.7) at room temperature.

Secondary ion mass spectroscopy (SIMS) analyses were performed to study the chemical nature of the corrosion products deposited around the α-Al(Fe,Mn)Si phase particles after a few hours of immersion in deionised water. SIMS maps were acquired on a Cameca IMS 4F/6F apparatus. The samples were sputtered on a window of 500 μm × 500 μm using O^{2-} ions as primary beam with a current of 200 nA. The maps were obtained for areas of 150 μm × 150 μm using a 50 pA O^{2-} ions beam. Four signals were collected during the analysis: 27 Al, 28 Si, 55 Mn and 56 Fe. High-resolution mode was used to avoid interference between the different signals.

3. Results and discussion

The electrochemical measurements presented in this section suggest a form of defective passivation that is caused by heterogeneities in the aluminium matrix. The global electrochemical measurements were supported by use of microscopic techniques to explore the reactivity of individual particles.

3.1. Electrochemical measurements

The polarisation curves for the residual cladding in 0.1 M Na_2SO_4 are presented in Fig. 3. Fig. 3(a) presents the curves plotted without EG for three temperatures and Fig. 3(b) shows the results obtained at 90 °C in various water–EG mixtures. The curves obtained without EG (Fig. 3(a)) show a slight evolution of the cathodic current densities when the temperature increases. The plateau observed is attributed to oxygen reduction and the current densities are between 3×10^{-5} and 3×10^{-4} A cm^{-2}. Concerning the anodic branch, a progressive increase of the current density with potential is observed. This indicates that passivation of the residual cladding is not obtained in a 0.1 M Na_2SO_4 aqueous solution whatever the temperature in the range 10–90 °C. The anodic curves obtained for the three temperatures are parallel indicating that the mechanism is independent of temperature. The increase of the temperature enhances the rate of the process. This anodic behaviour is neither passivation nor pitting corrosion. As the increase of the current density with increasing potential is small and the values reached not very high, it is assumed that this behaviour is associated with the presence of defective sites in the passivation film covering the alloy. Consequently, this anodic behaviour is called

"defective passivation" for the remainder of the study. As a consequence of the cathodic and anodic behaviour, the corrosion potential (E_{corr}) is shifted in the cathodic direction when the temperature increases. At 90 °C, when the EG content increases (Fig. 3(b)), a decrease of both the cathodic and the anodic current densities is observed. The cathodic current density is not clearly explained due to the complex evolutions of both the oxygen solubility and the viscosity in water–EG mixtures as a function of the temperature. The anodic curve tends toward a plateau when the EG content becomes higher than 60%. This last anodic behaviour indicates the surface passivation of the residual cladding. Consequently, the addition of ethylene glycol seems to favour a transition from defective passivation to passivation for the residual cladding. As an opposite effect of the temperature increase, the EG content increase shifts E_{corr} in the anodic direction.

Fig. 3. Polarisation curves for the residual cladding plotted in aerated 0.1 M Na_2SO_4 solutions (a) without EG for three temperatures: (■) 10 °C, (□) 50 °C and (●) 90 °C and (b) in different water–EG mixtures at 90 °C: (●) 0% EG, (□) 30% EG, (■) 60% EG, (○) 80% EG.

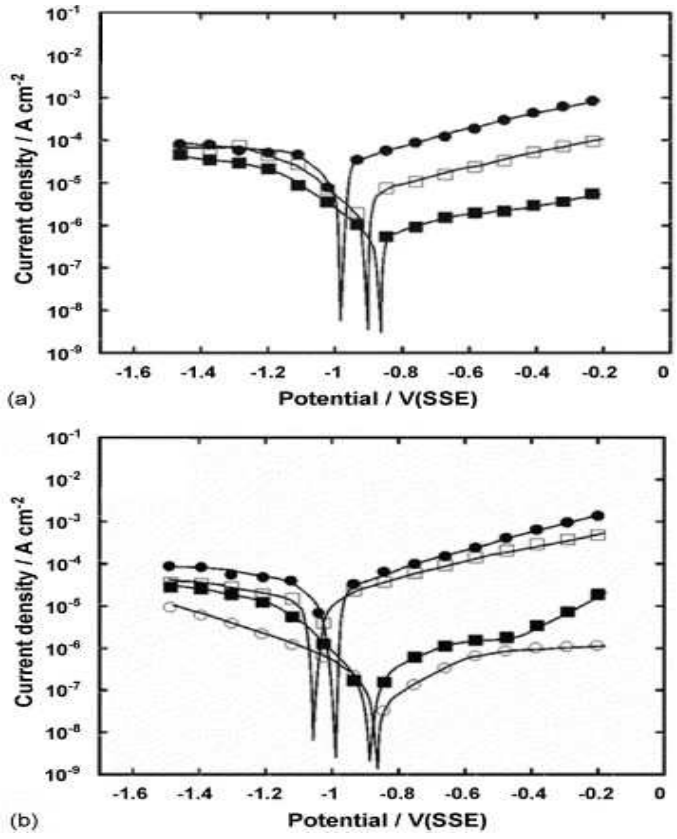

The polarisation curves plotted in 0.1 M Na_2SO_4 + 0.01 M NaCl solutions are presented in Fig. 4. Fig. 4(a) presents the curves obtained without EG for three temperatures whereas Fig. 4(b) shows the curves plotted at 90 °C in different water–EG mixtures. The addition of 0.01 M of chloride ions (Fig. 4(a) and (b)) does not change the cathodic current densities by comparison with those measured in 0.1 M Na_2SO_4 solution. Although E_{corr} is shifted toward the cathodic potentials with chloride addition, its decrease with temperature increase and with EG content decrease is similar to that observed without chlorides (Fig. 3(a) and (b)). The first anodic domain between E_{corr} and −0.95 V/SSE is similar to that obtained without chloride (passivation or defective passivation), but at potentials higher than −0.95 V/SSE, the curves are extended by a strong increase of the current density associated to pitting. As a consequence, when E_{corr} is close to −0.95 V/SSE, such as for water at 10 °C or 80% EG mixture at 90 °C, pitting potential and corrosion potential are superimposed. These results show that the presence of chloride can induce an additional electrochemical behaviour, *i.e.* pitting corrosion, for the residual cladding at E_{corr} in specific conditions. It is interesting to note that pitting corrosion occurs at the corrosion potential when chloride ions are added to the solution in experimental conditions where the material presents the best corrosion resistance in 0.1 M Na_2SO_4 solution without chlorides (low temperature and/or high EG content).

Fig. 4. Polarisation curves for the residual cladding plotted in aerated 0.1 M Na_2SO_4 + 0.01 M NaCl solutions (a) without EG for three temperatures: (■) 10 °C, (□) 50 °C and (●) 90 °C and (b) in different water–EG mixtures at 90 °C: (●) 0% EG, (□) 30% EG, (■) 60% EG, (○) 80% EG.

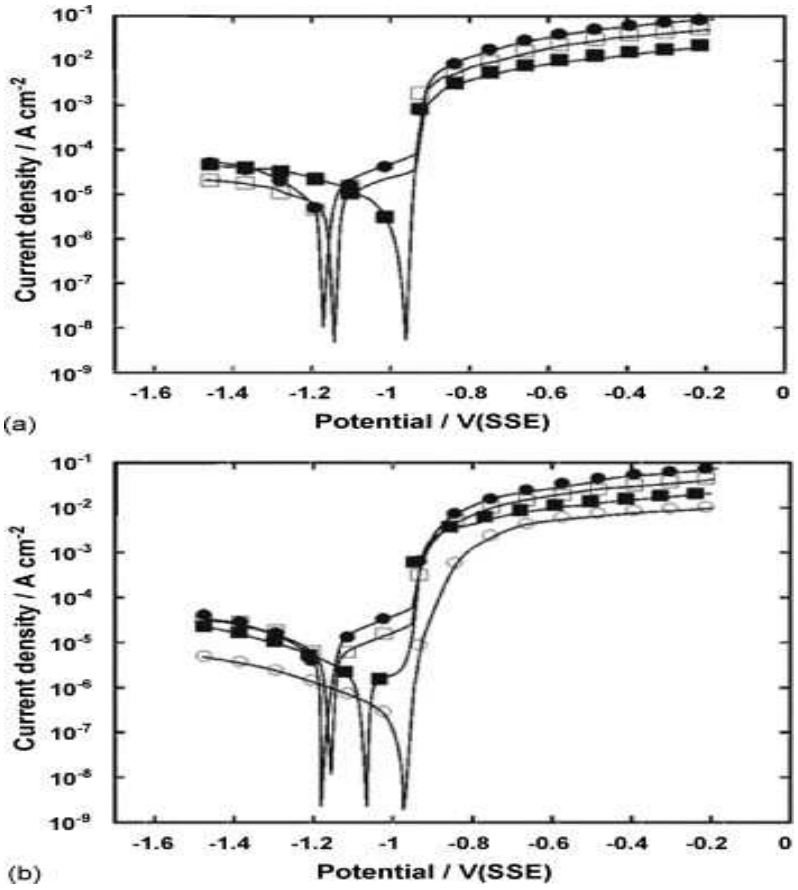

The particular cases where pitting potential and corrosion potential are the same on the polarisation curves were analysed by OM observations after 150 h of immersion. A few large pits were observed on the sample immersed at 10 °C in water containing 0.1 M Na_2SO_4 + 0.01 M NaCl. Conversely, many small pits were observed in the valleys on the sample immersed at 90 °C in the 80% EG solution containing 0.1 M Na_2SO_4 + 0.01 M NaCl. These results confirm the susceptibility of the residual cladding to pitting corrosion when it is immersed in these particular conditions since no pits were observed in the other conditions. However, the differences observed concerning the density and the size of the pits requires further investigations. The study was rather focused on the defective passivation behaviour

encountered in many conditions and with the transition from passivation to defective passivation. However, it would also be interesting to determine whether the initiation sites of the pits correspond to weak points inducing the transition from passivation to defective passivation.

Among the three electrochemical behaviours evidenced for the residual cladding at E_{corr}, *i.e.* passivation, defective passivation and pitting, the reasons for the defective passivation observed in many cases are investigated in greater depth. For comparison, the polarisation curves of pure aluminium were plotted in different 0.1 M Na_2SO_4 water–EG mixtures with and without 0.01 M NaCl at different temperatures. Two examples are presented in Fig. 5 for EG-free solutions. It is clear that passivation is obtained at E_{corr} for pure aluminium with and without chlorides. Since the main difference between pure Al and the residual cladding is the presence of Si needles and of particles of α-Al(Fe,Mn)Si phase, the defective passivation can arise from the presence of these heterogeneities.

Fig. 5. Polarisation curves for pure aluminium plotted at 30 °C in aerated EG-free solutions containing 0.1 M Na_2SO_4 (■) and 0.1 M Na_2SO_4 + 0.01 M NaCl (□).

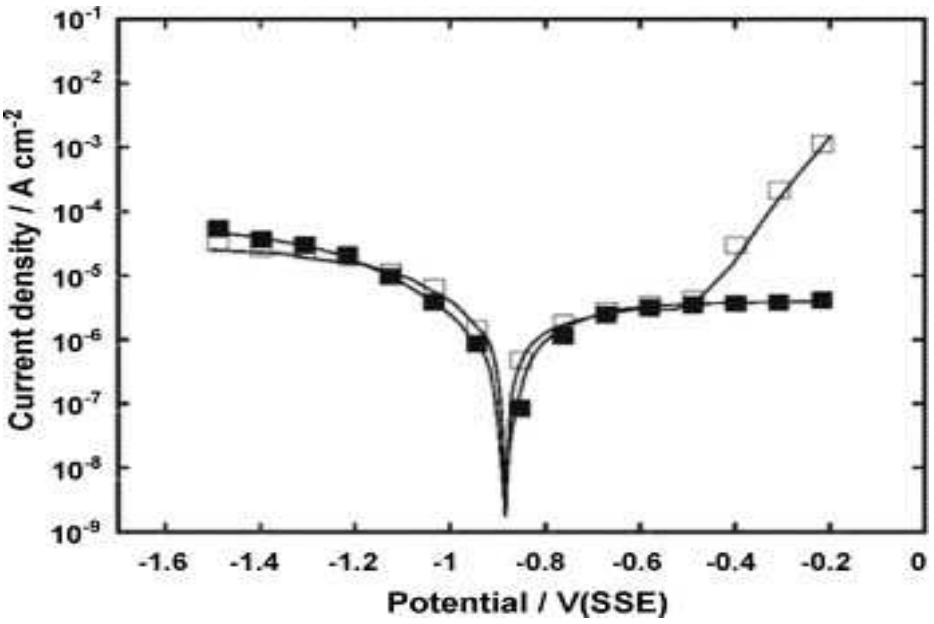

3.2. Phase shifting interferometric microscopy

PSIM was used to clarify the role of heterogeneities on the local electrochemical behaviour. Electrochemical measurements showed that the defective passivation was favoured when EG content was low in the mixture. Thus, immersion tests were performed in deionised water without any additives (pH 5.7) at room temperature. Fig. 6 presents 3D profiles of polished areas containing Si needles (Fig. 6(a) and (b)) and a α-Al(Fe,Mn)Si phase particle (Fig. 6(c) and (d)) before and after immersion. Due to their greater hardness by comparison with the (Al) matrix, silicon needles and the α-Al(Fe,Mn)Si particle appear in relief on the profiles, just after polishing. Comparison of the profiles of the sample containing Si needles before and after immersion (Fig. 6(a) and (b)) did not reveal significant modifications of the surface, independently of the hold time in water. This suggests that the defective passivation of the residual cladding is not linked to the presence of the Si needles. The trend of the profiles obtained around α-Al(Fe,Mn)Si particle (Fig. 6(c) and (d)) is strongly modified by immersion. The dissolution of the precipitate and of the surrounding (Al) matrix is observed after immersion (Fig. 6(d)). These observations show that the defective state of the passivation probably arises from a reactivity of the α-Al(Fe,Mn)Si particles or between the α-Al(Fe,Mn)Si particles and the (Al) matrix.

Fig. 6. 3D PSIM profiles of areas containing Si needles (a and b) and a α-Al(Fe,Mn)Si phase particle (c and d) before immersion (a and c), and after 90 min of immersion in deionised water at room temperature (b and d).

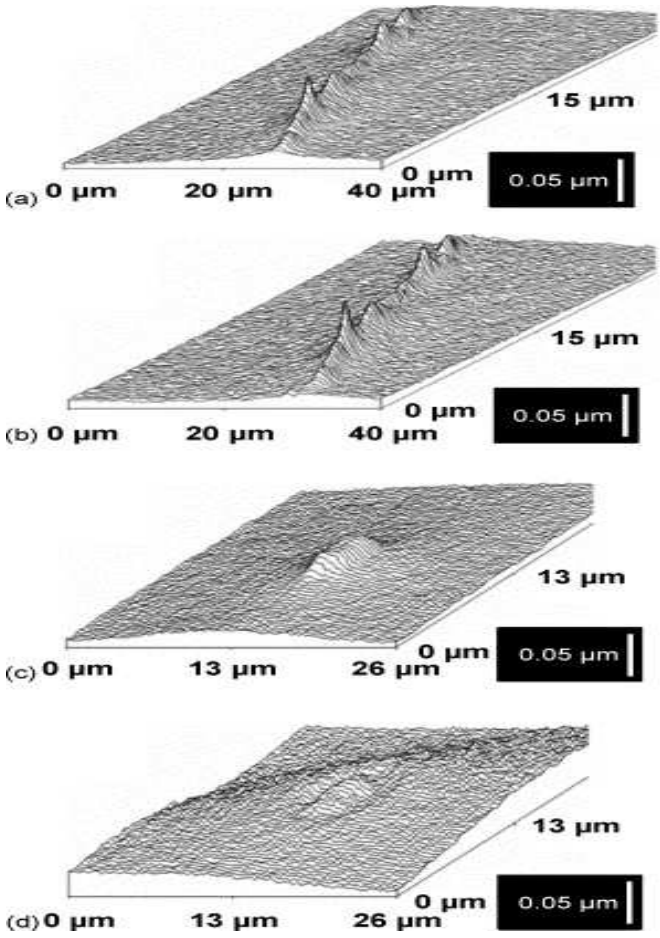

3.3. Particles/matrix interactions

OM and SEM observations of the residual cladding were performed after various exposure times in deionised water to follow the initiation of corrosion. Fig. 7 presents three OM observations of the surface of the residual cladding before and after short immersion durations (1 and 3 h) and a SEM micrograph obtained after a longer exposure time (150 h). During the first hours (Fig. 7(b) and (c)), brown corrosion products (in grey on the micrographs) coming from the α-Al(Fe,Mn)Si/Al interface deposit on the aluminium matrix around the precipitate.

It is noteworthy that these corrosion products were also observed after anodic polarisation in the Na_2SO_4 solution. For longer exposure time, this deposition of corrosion products is followed by the corrosion of the aluminium matrix which starts around the α-Al(Fe,Mn)Si particle (Fig. 7(c)). Finally, after 150 h (Fig. 7(d)), the α-Al(Fe,Mn)Si precipitate remains little attacked whereas the surrounding aluminium is strongly corroded. This last observation may signify that an inversion of the polarity between the α-Al(Fe,Mn)Si phase particles and the surrounding aluminium matrix occurs after several hours of immersion in water. This sequence of reactivity is representative of the electrochemical behaviour of most of the particles. Previous metallurgical studies [1] and [2] revealed variations of Fe and Mn content of the α-Al(Fe,Mn)Si phase particles. However, the variation of particles composition is small when compared to the difference of composition between particles and the aluminium matrix. Consequently, they exhibit comparable electrochemical behaviour when they are embedded in the aluminium matrix.

Fig. 7. Optical microscope (a–c) and scanning electron microscope (15 kV, Wd = 19 mm) (d) observations showing the reactivity of the α-Al(Fe,Mn)Si particle/matrix couple after various immersion durations in deionised water at room temperature: (a) 0 h, (b) 1 h, (c) 3 h and (d) 150 h.

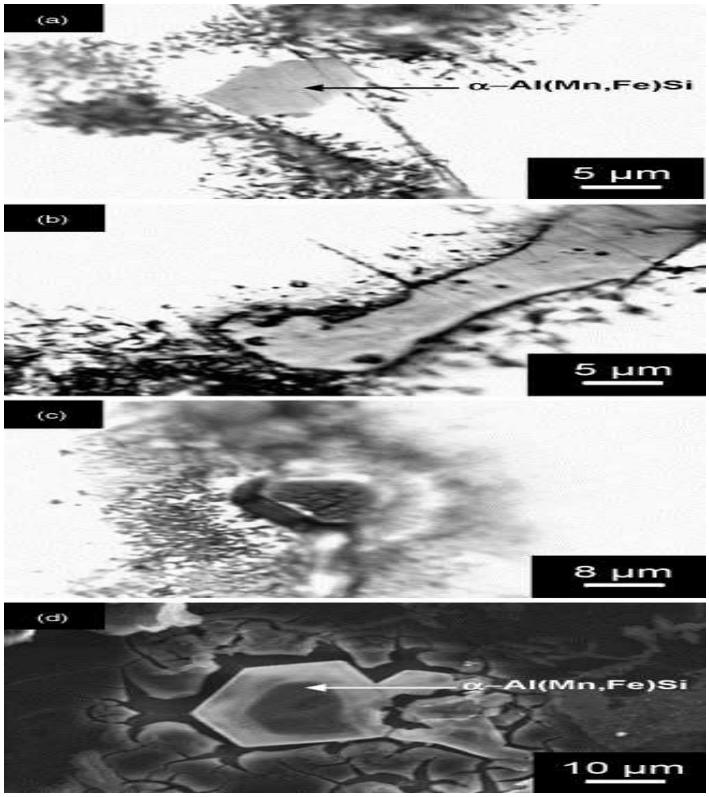

Electrochemical measurements were performed on isolated α-Al(Fe,Mn)Si particles in order to clarify the inversion of polarity inferred from microscopy observation. The plot of the anodic polarisation curves for the α-Al(Fe,Mn)Si particles at 30 °C in a 0.1 M Na_2SO_4 aqueous solution is presented in Fig. 8 and compared with the curves obtained for pure aluminium and for the residual cladding in the same conditions. The corrosion potential of the α-Al(Fe,Mn)Si particles (−1.08 V/SSE) is lower than both those of pure aluminium (−0.88 V/SSE) and the residual cladding (−0.95 V/SSE). The anodic current densities are about a hundred times higher for the α-Al(Fe,Mn)Si particles than for the residual cladding and about thousand times higher than for pure aluminium. The ratio of about hundred between the anodic current densities of the residual cladding and of the α-Al(Fe,Mn)Si particles is in good agreement with the proportion of α-Al(Fe,Mn)Si precipitates in the residual cladding (about 1% of the total surface area). Thus, the increase of the current density with the potential observed for the residual cladding can be related to the reactivity of the α-Al(Fe,Mn)Si particles. It is also noteworthy that the corrosion potential of the residual cladding is between those of pure aluminium and of the α-Al(Fe,Mn)Si particles corroborating the major influence of these two phases on the electrochemical behaviour of the brazed material.

Fig. 8. Polarisation curves for pure aluminium (■), residual cladding (●) and the α-Al(Fe,Mn)Si phase particles (○) plotted in aerated 0.1 M Na_2SO_4 aqueous solution at 30 °C.

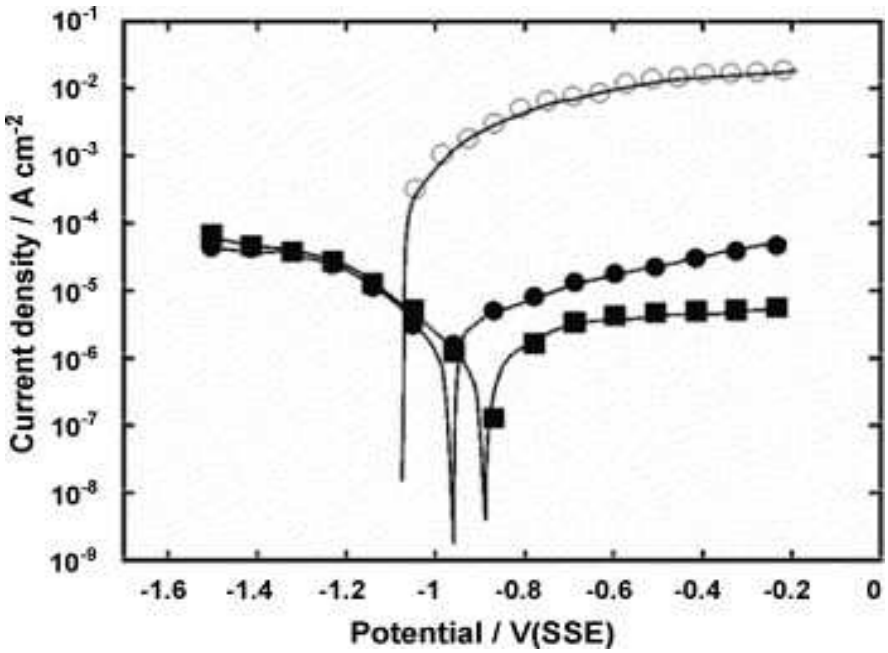

The oxidation state of the α-Al(Fe,Mn)Si particles at the corrosion potential of the brazed material evidenced from the polarisation curves presented in Fig. 8 is in good agreement with the observations carried out after a few hours of immersion in water. Identification of the elements present in the brown corrosion products deposited around the α-Al(Fe,Mn)Si phase particles during this first step was performed by SIMS. For this analysis, the samples were brazed without Nocolok® fluxing to avoid contamination of the surface by elements such as K, F, Na, Ca and Fe. After 5 s of sputtering, analyses were carried out on the first atomic layers of the surface for both a fresh sample and a sample immersed for 10 h in deionised water at room temperature. Fig. 9 shows maps obtained for Al, Si, Mn and Fe. Since the different elements do not react similarly to ionic bombardment, the maps must be compared element by element. The darker the area on the map, the lower the content of the element in that area. It appears that the superficial layer of the immersed sample (Fig. 9(b)) contains higher levels of Si, Mn and Fe than the fresh one (Fig. 9(a)). After further sputtering of 45 s (not shown), the analysis revealed a similar distribution of the elements for both samples corroborating that the high Si, Mn and Fe contents measured on the surface of the immersed sample were due to the deposition of the brown corrosion products. This reveals that the layer of brown corrosion products contains all the alloying elements of the α-Al(Fe,Mn)Si phase, probably under an oxidised form. As a consequence, the first step of the corrosion of the residual cladding is linked to the oxidation of the α-Al(Fe,Mn)Si particles particularly, at the particle/matrix interface.

Fig. 9. Secondary ion mass spectroscopy maps of the surface of the residual cladding showing the elements Al, Si, Mn and Fe in the first atomic layers of the surface for the freshly brazed material (a) and for the sample immersed during 10 h in deionised water (b).

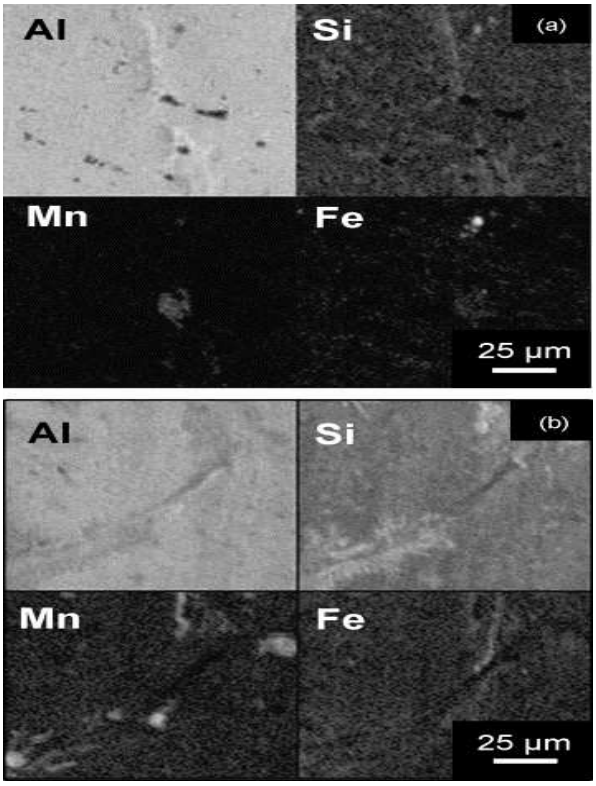

Although these experiments clarified the first steps of the corrosion mechanism, they did not explain the inversion of polarity suggested by the microscope observations after immersion in deionised water. The influence of the immersion duration in water was investigated following the open circuit potential as a function of immersion time for pure aluminium and for the α-Al(Fe,Mn)Si particles respectively during 140 and 160 h in aerated 0.1 M Na_2SO_4 aqueous solution at 30 °C. The results, presented in Fig. 10, confirm the tendency drawn from the polarisation curves with the stabilisation of the potential of the α-Al(Fe,Mn)Si particles at a lower value than that of pure aluminium, respectively, −1.08 and −0.91 V/SSE. These results suggest that the ageing of the α-Al(Fe,Mn)Si particles and pure aluminium taken separately in sodium sulphate solution does not explain the change of polarity assumed from the observations after immersion. The particle/matrix interactions need to be considered to understand the inversion of polarity. Considering the polarisation curves (Fig. 8), it can be observed that the α-Al(Fe,Mn)Si particles are submitted to anodic overvoltage when the brazed material is at E_{corr}. That means that the electrochemical behaviour of the particles

should evolve differently in the brazed material compared to when they are separated from the aluminium matrix.

Fig. 10. Open circuit potential vs. immersion time in aerated 0.1 M Na_2SO_4 aqueous solution at 30 °C for pure aluminium (■) and for the α-Al(Fe,Mn)Si phase particles (○).

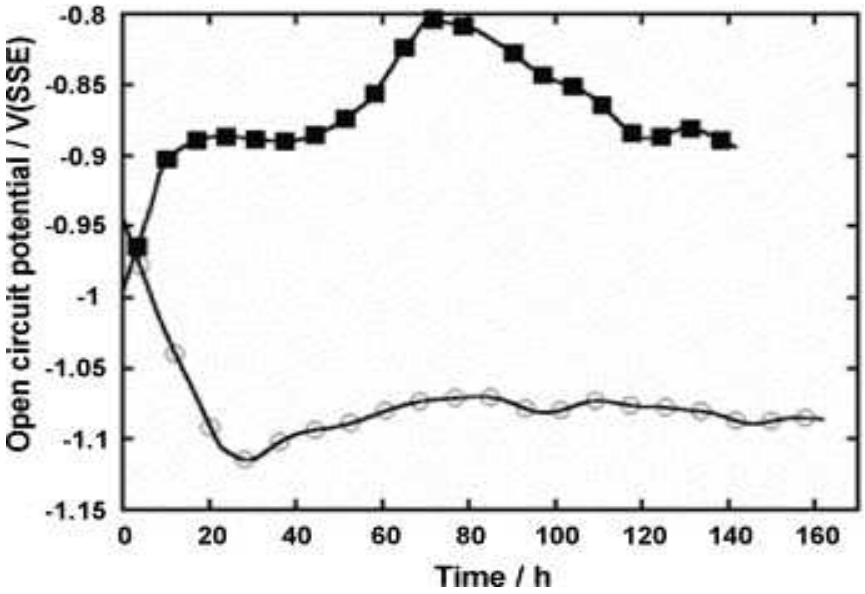

In order to simulate the particle/matrix interactions occurring in the brazed material, attempts at galvanic coupling between the electrode of α-Al(Fe,Mn)Si particles and a pure aluminium electrode were carried out. The electrode of α-Al(Fe,Mn)Si particles was used as working electrode in aerated 0.1 M Na_2SO_4 aqueous solution at 30 °C. Unfortunately, the results showed very low reproducibility. At the beginning, the α-Al(Fe,Mn)Si particles constituted the anode. Then, sometimes the coupling current stayed anodic, sometimes it became cathodic after a few minutes and sometimes the inversion of polarity occurred after several hours. These results suggest that the electrochemical behaviour of an intermetallic compound embedded in a matrix can hardly be simulated by a classical coupling setting. The modification of the surface occurring when corrosion products deposit on the surface of the material, the distribution of the electric field lines in the real configuration and the local pH

variations are not reproduced when the physical imbrication between the (Al) matrix and α-Al(Fe,Mn)Si particles does not exist. The quantitative proof of the change of polarity observed between the α-Al(Fe,Mn)Si phase particles and the (Al) matrix probably requires the use of local techniques such as local electrochemical impedance spectroscopy or scanning electrochemical microscopy which may allow to study in situ the particle/matrix interactions.

It was shown in Fig. 3(b) that the EG content had a strong influence on the electrochemical behaviour of the residual cladding and more particularly, that the defective passivation became passivation for high EG contents in the absence of chloride ions. The addition of EG on the reactivity of the α-Al(Fe,Mn)Si particles was studied by OM observations (not shown) of the residual cladding surface after 10 h of immersion in different water–EG mixtures (0, 25, 50, 55, 75 and 100% EG). Without EG, the observations revealed features similar to those obtained after 3 h of immersion (Fig. 7(c)) with the presence of brown corrosion products around the precipitates. With the increase of the EG content, the quantity of brown products deposited around the precipitates decreased. For EG contents equal to or higher than 55%, brown corrosion products were no longer observed. This indicates that the dealloying of the α-Al(Fe,Mn)Si phase particles observed in water-rich water–EG mixtures does not occur in EG-rich water–EG mixtures. The α-Al(Fe,Mn)Si phase particles are not reactive sites in these conditions and are not prone to oxidise or to become cathodic sites. Finally, in these conditions, both the (Al) matrix and α-Al(Fe,Mn)Si particles are passive.

4. Conclusions

The corrosion behaviour of the residual cladding was investigated by plotting the polarisation curves in different neutral media representative of the cooling liquids. Three types of electrochemical behaviour depending on the experimental conditions were evidenced: (i) passivation, (ii) defective passivation characterised by a slow increase of the current densities with the potential and (iii) pitting corrosion at the corrosion potential. In low EG content mixtures and/or at high temperature, the defective passivation was often observed. The results have shown that the Si needles do not participate in this depassivation. Conversely, reactivities occur at the α-Al(Mn,Fe)Si phase particles level. During the first hours of immersion, the α-Al(Mn,Fe)Si particles are the only ones to react. Deposition of the

alloying elements Mn, Fe and Si occurs around the particles, probably in an oxidised state. Then, the corrosion of the α-Al(Mn,Fe)Si particles stops whereas the surrounding (Al) matrix dissolves. The presence of EG decreases the reactivity of the α-Al(Mn,Fe)Si particles to such an extent that it is stopped for EG content higher than 55% (passivation plateaus on the polarisation curves). It is noteworthy that pitting corrosion occurs in the presence of chloride ions in some particular conditions but these cases need further investigations. The following studies focus on the propagation of the corrosion through the brazed material.

Acknowledgement

This work was carried out with financial and technical support from Valeo Engine Cooling (La Suze sur Sarthe, France)

References

S. Tierce, N. Pébère, C. Blanc, G. Mankowski, H. Robidou, D. Vaumousse and J. Lacaze, *Int. J. Cast Met. Res.* 18 (2005) (6), p. 370.

J. Lacaze, S. Tierce, M.-C. Lafont, Y. Thebault, N. Pébère, G. Mankowski, C. Blanc, H. Robidou, D. Vaumousse and D. Daloz, *Mater. Sci. Eng. A* 413–414 (2005), p. 317.

ASM international (8th ed.), *Metals Handbook, Welding and Brazing* vol. 6, ASM international (1971), p. 675.

D.P. Sekulic, *Int. J. Eng. Sci.* 39 (2001), p. 229.

D.P. Sekulic, B.J. Zellmer and N. Nigro, *Model. Simul. Mater. Sci. Eng.* 9 (2001), p. 357.

B.J. Zellmer, N. Nigro and D.P. Sekulic, *Model. Simul. Mater. Sci. Eng.* 9 (2001), p. 339. M. Nylen, U. Gustavsson, B. Hutchinson and A. Ortnas, *Aluminium alloys: Conference Proceedings of ICAA5 on Materials Science Forum, vols. 217–222* Trans.Tech. Publication, Zurich, Switzerland (1996), p. 1703.

R.A. Woods, *VTMS3: Conference Proceedings of Vehicle Thermal Management Systems Congress* SAE, Warrendale, USA (1997), p. 639 paper No 971848.

H.J. Yang and R.A. Woods, *VTMS3: Conference Proceedings of Vehicle Thermal Management Systems* SAE, Warrendale, USA (1997), p. 649 paper No 971849.

G.J. Marshall, R.K. Bolingbroke and A. Gray, *Met. Trans. A* 24 (1993), p. 1935.

R. Benedictus, S.D. Meijers, A.J. Wittebrood and J.H.W. de Witt, *Aluminium alloys: Conference Proceedings of ICAA6* The Japan Institute of Light Metals, Toyohashi, Japan (1998), p. 1577.

A.C. Scott, R.A. Woods and J.F. Harris, *SAE: Conference Proceedings of SAE international Congress* SAE, Warrendale, USA (1991) paper No 910590.

Y. Isobe, K. Takeuchi, M. Tanaka, M. Mori, S. Yamauchi and K. Namba, *SAE: Conference Proceedings of SAE international Congress* SAE, Warrendale, USA (1993) paper No 930149.

F.M. Al-Kharafi and W.A. Badawy, *Electrochim. Acta* 40 (1995), p. 1811.

S.S. Abdel Rehim, H.H. Hassan and M.A. Amin, *Corros. Sci.* 46 (2004), p. 1921.

S. Kuroda and K. Tohma, *Aluminium Alloys: Conference Proceedings of ICAA6* The Japan Institute of Light Metals, Toyohashi, Japan (1998), p. 1543.

S. Meijers, PhD Thesis, 2002, ISBN 90-805661-3-6.

K. Nisançiöglu, *J. Electrochem. Soc.* 137 (1990), p. 69.

K. Nisançiöglu and O. Lunder, *Aluminium Alloys: Conference Proceedings of ICAA1* Chameleon Press, London, Great Britain (1986), p. 1125.

M. Pourbaix, Atlas des équilibres électrochimiques, Gauthier-Villars et Cie Ed., Paris, France, 1963.